Letter

Two-dimensional electron gas at the (001) surface of ferromagnetic $EuTiO_3$

R. Di Capua,[1,2,*] M. Verma,[3] M. Radović,[4] N. C. Plumb,[4] J. H. Dil,[4,5] Z. Ristić,[6] E. B. Guedes,[4,5] G. M. De Luca,[1,2] D. Preziosi,[7] Z. Wang,[4] A. P. Weber,[4,5] R. Pentcheva,[3] and M. Salluzzo[2,†]

[1]*Dipartimento di Fisica "Ettore Pancini" Università di Napoli "Federico II", Complesso Monte-Santangelo via Cinthia, I-80126 Napoli, Italy*

[2]*CNR-SPIN Complesso Monte-Santangelo via Cinthia, I-80126 Napoli, Italy*

[3]*Department of Physics and Center for Nanointegration (CENIDE), Universität Duisburg-Essen, Lotharstr. 1, 47057 Duisburg, Germany*

[4]*Photon Science Division, Paul Scherrer Institut, 5232 Villigen PSI, Switzerland*

[5]*Institute of Physics, École Polytechnique Fédérale de Lausanne, 1015 Lausanne, Switzerland*

[6]*Vinča Institute of Nuclear Sciences, 11000 Belgrade, Serbia*

[7]*Université de Strasbourg, CNRS, IPCMS UMR 7504, 67034 Strasbourg, France*

(Received 23 December 2020; accepted 25 October 2021; published 10 December 2021)

Studies on oxide quasi-two-dimensional electron gas (q2DEG) have been a playground for the discovery of novel and sometimes unexpected phenomena, like the reported magnetism at the surface of $SrTiO_3$ (001) and at the interface between nonmagnetic $LaAlO_3$ and $SrTiO_3$ band insulators. However, magnetism in this system is weak and there is evidence of a nonintrinsic origin. Here, by using *in situ* high-resolution angle-resolved photoemission, we demonstrate that ferromagnetic $EuTiO_3$, the magnetic counterpart of $SrTiO_3$ in the bulk, hosts a q2DEG at its (001) surface. This is confirmed by density functional theory calculations with Hubbard U terms in the presence of oxygen divacancies in various configurations, all of them leading to a spin-polarized q2DEG related to the ferromagnetic order of Eu-4f magnetic moments. The results suggest $EuTiO_3$(001) as a new material platform for oxide q2DEGs, characterized by broken inversion and time-reversal symmetries.

DOI: 10.1103/PhysRevResearch.3.L042038

The discovery of a surface/interfacial quasi-two-dimensional electron gas (q2DEG) in $SrTiO_3$ [1–3] boosted expectations for novel oxide electronics due to the intriguing and rich physics uncovered, including multiband and possibly unconventional superconductivity [4–6], large spin-orbit coupling (SOC) [7] and large spin to charge conversion efficiency [8]. While magnetic effects were reported [9], several studies attributed them to weak-(para)magnetism induced by extrinsic defects, such as oxygen vacancies [10].

$EuTiO_3$ (ETO) is an antiferromagnetic (AFM) insulator isostructural to $SrTiO_3$ (STO). Like STO, it is characterized by empty Ti-3d bands. In contrast to STO, however, Eu^{2+} magnetic moments order antiferromagnetically below 5.5 K and form a spin-polarized band 2 eV below the Fermi level with 4f orbital character. The AFM order reverts into a ferromagnetic (FM) one (T_c = 6–8 K) by doping or lattice strain [11,12]. Due to combined effects of SOC and spontaneous Zeeman field, doped-ETO exhibits a bulk band structure with Weyl nodes and a topological Hall effect [13,14]. These exotic properties may induce intriguing physical phenomena in confined q2DEGs at the ETO surfaces and interfaces.

Here, by employing angular resolved photoemission spectroscopy (ARPES) on *in situ* grown thin films, we show that the (001) surface of ferromagnetic ETO hosts a q2DEG. Density functional theory calculations with Hubbard U terms (DFT + U) suggest a spin-polarized q2DEG related to the FM order of Eu-4f magnetic moments.

We studied ETO films with thickness of 2, 5, and 15 unit cells (uc) deposited *in situ* by reflection high-energy electron diffraction assisted pulsed laser deposition on TiO_2-terminated (001) STO single crystals at the Surface/Interface Spectroscopy (SIS) beamline of the Swiss Light Source (Fig. S1, Ref. [15]). We also studied a 15-uc ETO sample deposited on a $SrRuO_3$ buffer layer to improve ground contact. After the deposition, the samples were annealed in ultrahigh vacuum (UHV) at 600 °C for one hour and then *in situ* transferred to SIS ARPES end-station. The UHV annealing does not perturb the 1×1 surface structure, as confirmed by low energy electron diffraction (Fig. S1 [15]). X-ray diffraction shows that the ETO films grow coherently, with almost no strain, and have a lattice constant (3.92 ± 0.01 Å), close to that of bulk STO (Figs. S1(d)–S1(f) [15]). Finally x-ray magnetic dichroism and SQUID magnetometry data show that the films are ferromagnetic with a $T_c < 10$ K and a magnetic moment close to the value of 7 μ_B/Eu expected for Eu^{2+} (Fig. S2 [15]).

The ETO surface state was compared to STO-qDEGs with a controlled 2D carrier density n_{2D} created either by mild Ar^+ sputtering and low pressure oxygen annealing(STO-A), or just by UHV annealing (STO-B) of TiO_2 terminated (001) STO single crystals [16,17]. To assess the nature of the (001) ETO surface state, in Fig. 1, we report in-plane momentum

*roberto.dicapua@unina.it

†marco.salluzzo@spin.cnr.it

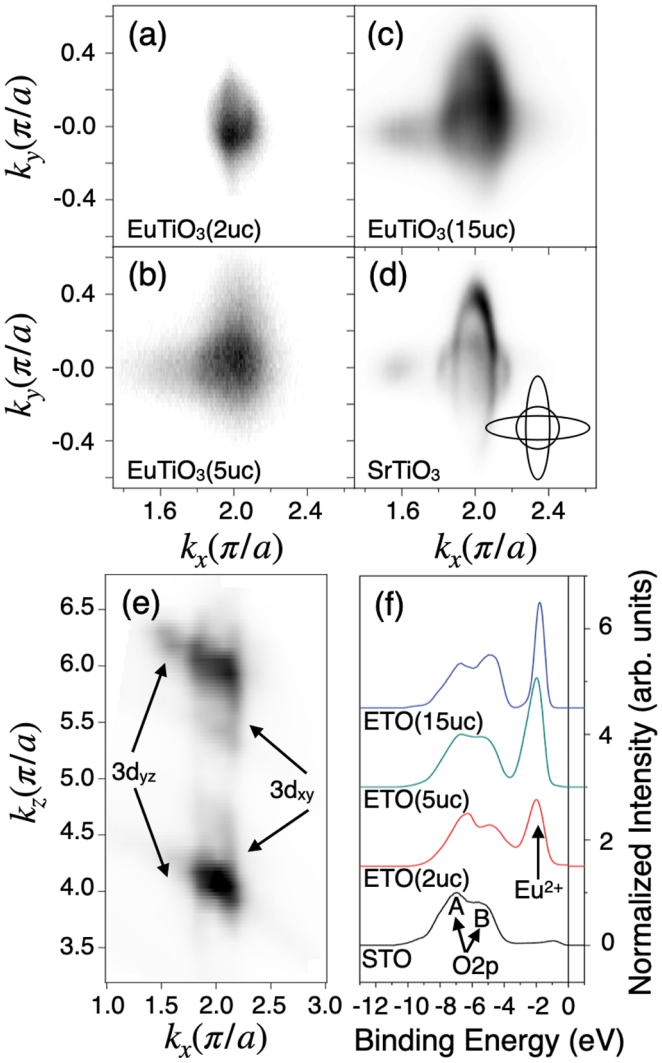

FIG. 1. [(a)–(d)] FS in the second Brillouin zone measured with an incoming photon energy of 85 eV and C + polarization: (a) 2-uc ETO, (b) 5-uc ETO, (c) 15-uc ETO and (d) STO samples. In the inset of (d), we show a sketch of the FS based on independent t_{2g}-states bands. (e) k_x-k_z cut measured on the 15-uc ETO showing the two-dimensional dispersing $3d_{xy}$ light band and the more 3D-like $3d_{yz}$ heavy band. (f) Angle integrated VB spectra on STO and ETO based q2DEGs. Features A and B indicate the O-2p band. A gradual inversion between the intensities of the A and B peaks going from STO to ETO films is related to the differences in the Sr-O-2p and Eu-O-2p hybridization in the two materials.

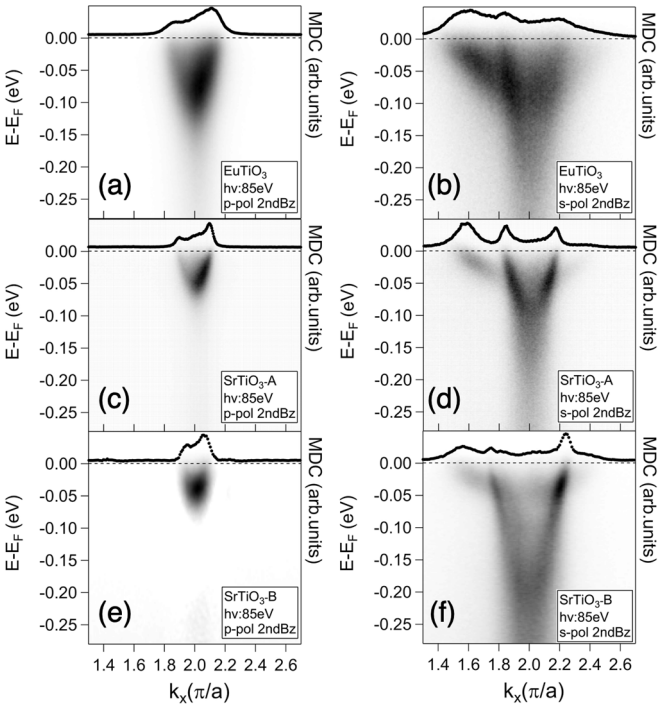

FIG. 2. High-resolution dispersion maps on STO and ETO (001) surfaces: second Brillouin zone k_x dispersion maps measured on 15-uc ETO [(a) and (b)], STO-A [(c) and (d)], and STO-B q2DEGs [(e) and (f)], with incoming photon energy of 85 eV. The corresponding MDCs at the Fermi level, integrated over an energy window of 10 meV around the Fermi level, are shown as traces (circles) on the top of each panel.

(k_x-k_y) Fermi surface (FS) cuts of 2- and 5-uc ETO films deposited on STO [Figs. 1(a) and 1(b)] of a 15-uc ETO film deposited on buffer $SrRuO_3$ [Fig. 1(c)] and of an STO single crystal [Fig. 1(d)]. Data were acquired at 15 K with photon energy $h\nu = 85$ eV, right-handed circular (C+) polarization and an out-of-plane k_z momentum close to the Γ_{103} reciprocal lattice point of the equivalent bulk periodicity [16–18]. FS maps show qualitatively similar features on the ETO and STO surface states: a circular ring centered on Γ and two ellipsoids elongated in k_x and k_y directions [inset of Fig. 1(d)]. Both structures are assigned to bands originating from t_{2g} Ti-3d states, the ring-shaped one corresponding to light effective mass electrons having main $3d_{xy}$ orbital character, and the ellipsoidal ones related to heavy effective mass electrons with main $3d_{xz}$-$3d_{yz}$ characters. We observe notable differences between 2-uc and thicker ETO films, which are reflected also in the band dispersions (Fig. S3 [15]), suggesting a contribution in 2-uc ETO from the underlying STO. Thus in the following we focus our analysis on 15-uc ETO, and in particular on 15uc ETO deposited on $SrRuO_3$ which has the best signal to noise ratio.

In Fig. 1(e), we show a k_x-k_z plane cut at $k_y = 0$ measured on the 15-uc ETO film by changing the incoming photon energy. The Fermi sheet corresponding to the light band has a nearly cylindrical shape with a k_z-independent 2D-character typical of a q2DEG, while the heavy bands show a k_z dispersion related to a more 3D-like character. These findings, similar to those observed on the (001) STO surface [16], demonstrate that ETO(001) hosts a q2DEG at its surface.

On the other hand, (001) ETO and STO surface states show important distinctive features. Figure 1(f) shows the evolution of the angle-integrated valence band (VB) spectra from reference STO q2DEG to (001) ETO thin films of different thicknesses. The data show in ETO the emergence of a Eu^{2+} narrow band, with a nondispersing character (Fig. S4 [15]), 1.95 eV below the Fermi level, related to localized $4f^7$ states.

To evaluate the main differences between the ETO and STO q2DEGs, in Fig. 2, we compare high statistics band dispersion, k_x cuts through Γ point, acquired with different

TABLE I. Effective masses (in units of electron mass) of the ETO and STO q2DEGs obtained from a tight-binding fit of the band dispersions and comparison with DFT+U calculations.

	From tight binding fit				DFT + U	
	$m_{xy}(k_F)$ [±0.05]	$m_{xy}(0)$ [±0.05]	$m_{xz}(k_F)$ [±0.05]	$m_{yz}(k_F)$ [±1]	$m_{xy}(0)$	$m_{yz}(k_F)$ FM/AFM
ETO	0.50	0.40	0.30	19	0.5	17.1/19.0
STO-A	0.60	0.50	0.50	23	0.6	22.2
STO-B	0.70	0.60	0.50	28		

linear polarizations on the 15-uc (001) ETO film [Figs. 2(a) and 2(b)] and on two (001) STO single crystals [Figs. 2(c) and 2(d) STO-A, Figs. 2(e) and 2(f) STO-B] having 2D carrier densities n_{2D} of $1.1 \pm 0.1 \times 10^{14}$ cm^{-2} (STO-A) and $1.4 \pm 0.1 \times 10^{14}$ cm^{-2} (STO-B), slightly below and above that of ETO ($n_{2D} = 1.3 \pm 0.1\ 10^{14}$ cm^{-2}). The band dispersion profiles were determined by fitting the intensity maxima of the momentum dispersion curves (MDCs) at different binding energies (Fig. S5 [15]); n_{2D} were estimated from the Luttinger volume of each band.

Through dipole selection rules we identify the bands in the *p-pol* maps of Fig. 2 (left panels) as the $3d_{xz}$ band observed along the "narrow"k diameter of the ellipse, while the bands observed in the *s-pol* maps (right panels) are light $3d_{xy}$ bands and heavy $3d_{yz}$ bands along the "wider"k diameter of the ellipse. Additional features in MDCs at the Fermi level suggest the presence of at least one additional light band located above the lowest $3d_{xy}$ band in both ETO and STO-B samples. The data show that the band bottom of the $3d_{xz}$ and $3d_{yz}$ heavy bands in the ETO q2DEG is substantially lower than the one measured in the two STO q2DEGs, independent on n_{2D}. Instead, the $3d_{xy}$ band band bottom in ETO is lower than the one of the STO-A and remarkably higher than in STO-B [Fig. 2(d)], where it reaches a value of −210 meV. Consequently, the splitting at the Γ point between the low lying heavy and light bands in ETO, of the order of 60 meV, is smaller than the one typically measured in high carrier density STO q2DEGs and in other titanates like $CaTiO_3$ [19]. A simple tight binding interpolation of the band features, assuming independent $3d_{xy}$, $3d_{xz}$ and $3d_{yz}$ bands, furnishes the effective masses in the different samples (Fig. S6 [15]). As shown in Table I, the ETO q2DEG is characterized by lower effective masses, compared to the STO surface states. Moreover, the band dispersions substantially deviate from the simple noninteracting tight-binding scenario for both STO and in particular ETO q2DEGs at the anticrossing point and near the Fermi level (Fig. S7 [15]).This implies a hybridization between t_{2g} bands with different symmetries, induced by crystalline distortion from octahedral environment and by the SOC, which naturally mixes the bands: consequently, while retaining some of the original orbital character, ETO conduction band electrons are characterized by coupled spin and orbital degrees of freedom, which could induce an exotic spin-orbit texture, with both in-plane and out-of-plane components. This affects the general charge and spin magneto-transport properties.

Since the conduction bands in ETO and STO are both formed by Ti-3d states, the question arises why the two q2DEGs show these differences and if the magnetic ordering of Eu^{2+}, demonstrated by magnetization data, could induce a spin polarization in the q2DEG. For these reasons we performed DFT + U calculations of STO and ETO (001) surfaces using the Vienna *ab initio* simulation package (VASP) [20,21] with the projector augmented wave (PAW) basis [22,23]. PBEsol exchange correlation functional [24] along with on-site Hubbard terms $U = 2$ eV for Ti-3d and $U = 7.5$ eV for Eu-4f states as implemented within the Dudarev's scheme [25] were used. The U value for Eu 4f is common for Eu-containing compounds and reproduces the position of the experimental Eu^{2+} peak in VB, while for Ti 3d, we used the typical value from literature [26,27]. The main results of the calculations are not strongly affected by the choice of U for Ti-3d states, although some details concerning the band dispersion and the position of the O-2p bands depend on this choice. The ionic positions were fully relaxed until the forces were less than 0.001 eV/Å.

Core-level spectroscopy suggests that ETO films are TiO_2 terminated [15]. Thus we show here DFT + U results for TiO_2 terminations, while in Ref. [15], we report calculations for EuO termination. Since ideal surfaces are insulating, we considered models containing an oxygen divacancy in various planar and vertical configurations, inducing the formation of a q2DEG [28,29]. In agreement with previous studies on STO(001) [28], we find that the most energetically favored configuration for both surfaces is a divacancy in a $2a \times 3a \times 4a$ supercell ($a = 3.905$ Å), with one missing oxygen in the topmost TiO_2 layer and a second in the subsurface Sr(Eu)O layer at a distance of 6.2 Å [Figs. 3(a) and 3(c)]. In the following, we show mostly results of the calculations performed using this configuration. Calculations of different magnetic configurations indicate that the FM solution is the most stable in both (001) STO and ETO, giving a localized Ti magnetic moment at the surface of about 0.12 μ_B/Ti. Figures 3(b), 3(e) (STO) and 3(d), 3(f) (ETO) show the spatial distribution of the q2DEG and of the Ti spin moment, together with the layer-, spin-, and element-resolved density of states (DOS) of the two systems. The O-2p VB extends from ∼−7 to −2.5 eV in both systems, while the spin polarized Eu-4f^7 orbitals appear in ETO(001) as a narrow (0.7 eV wide) band around −2 eV, in excellent agreement with experimental results. Above −1.5 eV the DOS contains contribution with predominant Ti-3d character and comprises the coexistence of localized states at −0.8 eV, in STO(001) surface only, as well as delocalized states in both ETO and STO surfaces contributing to the q2DEG.

To highlight the differences between the electronic band structure of (001) STO and ETO surface states, we show in Figs. 4(a)–4(c) and 4(d), 4(e) the spin-resolved band dispersions, calculated within the planar and vertical oxygen divacancy configurations, respectively, without including SOC. Further calculations including SOC are shown in Ref. [15]. The DFT + U results show that several bands cross E_F, the lowest lying one having a dispersive d_{xy} character switching along Γ-X direction into a much flatter band indicating an avoided crossing with the d_{xz}, d_{yz} bands. The higher lying bands around Γ are a combination of d_{xy} and d_{xz}, d_{yz} bands, comprising replicas from different layers due to the

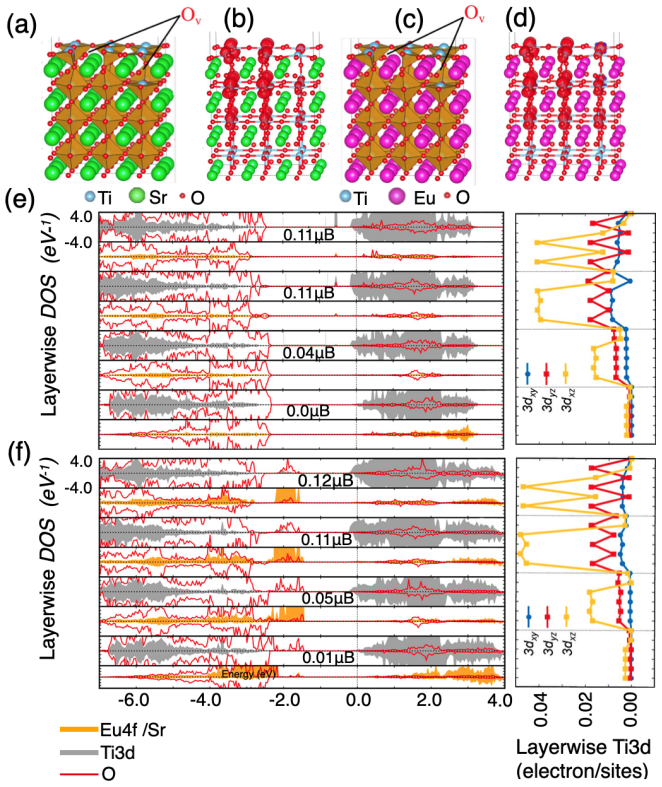

FIG. 3. Layer-, element-, and spin-resolved density of states of TiO_2-terminated ETO(001) and STO(001) surfaces from the DFT + U calculations: side views of the relaxed (a) STO(001) and (c) ETO(001) surfaces with an oxygen divacancy in the topmost TiO_2 layer and a second one in the subsurface SrO and EuO layers, respectively. (b) and (d) show the spin density (integrated between −0.4 eV and the Fermi level) with isovalues of 0.0005 $e/Å^3$. The color scale (blue to red) indicates predominant majority (red) spin contribution. (e) STO and (f) ETO layer-, spin-, and element- resolved density of states together with orbital-resolved Ti-3d occupation (electrons per site) showing the spatial distribution, the orbital polarization and Ti spin-magnetic moment of the q2DEGs.

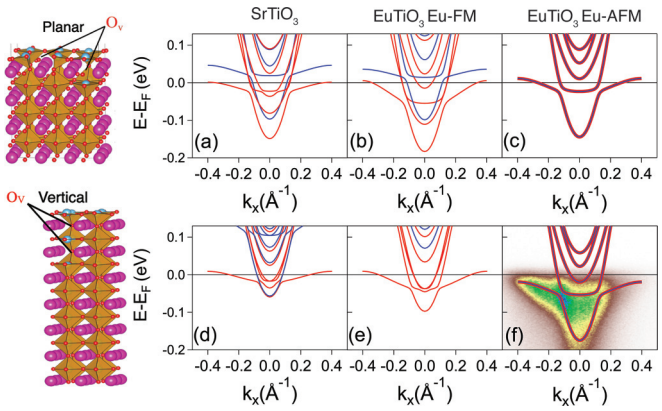

FIG. 4. Spin resolved band dispersions along Γ-X from the DFT + U calculations in the planar [(a)–(c)] and vertical [(d)–(e)] oxygen divacancy configurations without spin-orbit coupling (SOC) in STO(001) [(a) and (d)] and ETO(001) [(b), (c), and (e)]. On the left, we show also the supercells used in these calculations, with the location of the oxygen vacancies (O_V). For ETO(001), (b) and (c) show the band structure with Eu sublattice in FM and AFM order, respectively, highlighting how the FM order is crucial for the spin splitting. (f) A comparison between DFT + U in the AFM state of ETO (after a rigid band shift of −30 meV) and ETO band dispersion measured at 15 K with *s-pol* polarization. In each panel, the red and blue lines are spin-up (majority) and spin-down (minority) bands.

q2DEG confinement. In both planar and vertical oxygen divacancy configurations, overall, the bands in ETO(001) reach deeper below E_F compared to STO(001). The strong dispersion for the lowest lying band reflects in the effective masses around Γ (in both FM and G-AFM solutions, see Table I). In particular, within the FM planar oxygen divacancy configuration we find $m^* = 0.6\ m_e$ and $0.5\ m_e$ for STO(001) and ETO(001), respectively, versus $22.2\ m_e$ and $17.1\ m_e$ for the flat part along Γ-X. These values are in reasonable agreement with those extracted from ARPES data, confirming the experimental evidence of lower effective masses for the q2DEG at the (001) ETO surface. Moreover, DFT + U calculations correctly reproduce the overall downward shift of the heavy bands in the ETO(001) q2DEG. This downward shift is partly due to larger band-bending at the (001) ETO, due to the different lattice screening compared to (001) STO, and to a possible hybridization between Eu^{2+} and the conduction band. Indeed, the Eu^{2+} feature has a long tail merging with the quasiparticle peak, as shown in the energy distribution data (Fig. S4c [15]).

In both systems a spin splitting between majority (red) and minority (blue) bands emerges, however it is larger in ETO: ∼0.1 and ∼0.2 eV, for planar and vertical divacancy configurations, respectively. In STO(001) the largest spin splitting is ∼0.05 eV for the planar divacancy configuration, while almost spin-degenerate bands are found in the vertical oxygen divacancy configuration. We remark that the oxygen vacancies in the supercell calculations are long-range ordered, thus a prediction of a FM ground state in some configurations also in STO(001) is not surprising. However, the 1 × 1 lattice periodicity in experiment indicates that the oxygen vacancies are not ordered. This suggests that a FM q2DEG at the STO (001) surface can be obtained only by properly engineering the oxygen vacancies, maybe explaining some controversies among recent spin-resolved ARPES studies [30,31]. However, since ordered oxygen vacancies alone can lead to a spin-polarized q2DEG, one may wonder if the Eu^{2+} ferromagnetism is really necessary. In order to understand the role of Eu magnetism in the spin polarization of the q2DEG, in Fig. 4(c), we show that, for a G-AFM configuration, the Ti 3d bands are not spin-polarized. The AFM solution can be regarded as a first approximation of the paramagnetic state and, with a small rigid downward shift of 30 meV, it is in good agreement with the ARPES dispersion measured at 15 K, thus above the FM T_c. A direct experimental confirmation of a spin-polarized q2DEG at the ETO (001) surface would require a spin-resolved ARPES experiment below the FM T_c on a single domain of the FM-ETO surface state, which is unfeasible with the available setups. On the other hand, DFT + U predictions, and all the reported data suggest that the (001) surface of ferromagnetic

ETO hosts a spin-polarized oxide q2DEG, confirming recent experimental and theoretical studies on ETO [13,14,32] and (001) $LaAlO_3$/ETO/STO heterostructures [33]. In particular, DFT + U calculations show that the exchange interaction between Ti-3d states and ordered Eu^{2+} magnetic moments in the lattice is essential to create a spin-polarized q2DEG. We anticipate that other systems where a spin-polarized 2DEGs could be realized are $GdTiO_3$ [34] and $NdTiO_3$ [35], which are the magnetic counterpart of the $3d^1$ $LaTiO_3$ Mott insulator. The results presented in this work establish $EuTiO_3$ as a new material platform for oxide q2DEGs characterized by broken inversion and time-reversal symmetries, of interest for the study of novel quantum phenomena in low-dimensional systems.

This project received funding from the ERA-NET QUANTERA European Union's Horizon H2020 project QUANTOX under Grant Agreement No. 731473, the Ministero dell'Istruzione, dell'Universita e della Ricerca for the PRIN project TOP-SPIN (Grant No. PRIN 20177SL7HC), and the Swiss National Science Foundation (SNSF), Project No. 200021 182695. R.P. and M.V. acknowledge funding by the German Research Foundation (DFG) within CRC/TRR80 (Project No. 107745057, subproject G3) and CRC1242 (Project No. 278162697, subproject No. C02) and computational time at the Leibniz Rechenzentrum Garching, Project No. pr87ro and supercomputer magnitUDE (DFG Grants No. INST 20876/209-1 FUGG and No. INST 20876/243-1 FUGG).

[1] A. Ohtomo and H. Y. Hwang, A high-mobility electron gas at the $LaAlO_3/SrTiO_3$ heterointerface, Nature (London) **427**, 423 (2004).

[2] A. F. Santander-Syro, O. Copie, T. Kondo, F. Fortuna, S. Pailhes, R. Weht, X. G. Qiu, F. Bertran, A. Nicolaou, A. Taleb-Ibrahimi, P. Le Fevre, G. Herranz, M. Bibes, N. Reyren, Y. Apertet, P. Lecoeur, A. Barthelemy, and M. J. Rozenberg, Two-dimensional electron gas with universal subbands at the surface of $SrTiO_3$, Nature (London) **469**, 189 (2011).

[3] W. Meevasana, P. D. C. King, R. H. He, S.-K. Mo, M. Hashimoto, A. Tamai, P. Songsiriritthigul, F. Baumberger, and Z.-X. Shen, Creation and control of a two-dimensional electron liquid at the bare $SrTiO_3$ surface, Nat. Mater. **10**, 114 (2011).

[4] A. D. Caviglia, S. Gariglio, N. Reyren, D. Jaccard, T. Schneider, M. Gabay, S. Thiel, G. Hammerl, J. Mannhart, and J. M. Triscone, Electric field control of the $LaAlO_3/SrTiO_3$ interface ground state, Nature (London) **456**, 624 (2008).

[5] D. Stornaiuolo, D. Massarotti, R. Di Capua, P. Lucignano, G. P. Pepe, M. Salluzzo, and F. Tafuri, Signatures of unconventional superconductivity in the $LaAlO_3/SrTiO_3$ two-dimensional system, Phys. Rev. B **95**, 140502(R) (2017).

[6] G. Singh, A. Jouan, G. Herranz, M. Scigaj, F. Sanchez, L. Benfatto, S. Caprara, M. Grilli, G. Saiz, F. Couedo, C. Feuillet-Palme, J. LesueurDD, and N. Bergeal, Gap suppression at a Lifshitz transition in a multi-condensate superconductor, Nat. Mater. **18**, 948 (2019).

[7] A. D. Caviglia, M. Gabay, S. Gariglio, N. Reyren, C. Cancellieri, and J.-M. Triscone, Tunable Rashba Spin-Orbit Interaction at Oxide Interfaces, Phys. Rev. Lett. **104**, 126803 (2010).

[8] E. Lesne, Y. Fu, S. Oyarzun, J. C. Rojas-Sanchez, D. C. Vaz, H. Naganuma, G. Sicoli, J. P. Attane, M. Jamet, E. Jacquet, J. M. George, A. Barthelemy, H. Jaffres, A. Fert, M. Bibes, and L. Vila, Highly efficient and tunable spin-to-charge conversion through Rashba coupling at oxide interfaces, Nat. Mater. **15**, 1261 (2016).

[9] A. Brinkman, M. Huijben, M. Van Zalk, J. Huijben, U. Zeitler, J. C. Maan, W. G. Van der Wiel, G. Rijnders, D. H. A. Blank, and H. Hilgenkamp, Magnetic effects at the interface between non-magnetic oxides, Nat. Mater. **6**, 493 (2007).

[10] M. Salluzzo, S. Gariglio, D. Stornaiuolo, V. Sessi, S. Rusponi, C. Piamonteze, G. M. De Luca, M. Minola, D. Marre, A. Gadaleta, H. Brune, F. Nolting, N. B. Brookes, and G. Ghiringhelli, Origin of Interface Magnetism in $BiMnO_3/SrTiO_3$ and $LaAlO_3/SrTiO_3$ Heterostructures, Phys. Rev. Lett. **111**, 087204 (2013).

[11] T. Katsufuji and Y. Tokura, Transport and magnetic properties of a ferromagnetic metal: $Eu_{1-x}R_xTiO_3$, Phys. Rev. B **60**, R15021 (1999).

[12] J. H. Lee, L. Fang, E. Vlahos, X. Ke, Y. W. Jung, L. F. Kourkoutis, J.-W. Kim, P. J. Ryan, T. Heeg, M. Roeckerath, V. Goian, M. Bernhagen, R. Uecker, P. C. Hammel, K. M. Rabe, S. Kamba, J. Schubert, J. W. Freeland, D. A. Muller, C. J. Fennie *et al.*, A strong ferroelectric ferromagnet created by means of spin-lattice coupling, Nature (London) **466**, 954 (2010).

[13] K. S. Takahashi, H. Ishizuka, T. Murata, Q. Y. Wang, Y. Tokura, N. Nagaosa, and M. Kawasaki, Anomalous Hall effect derived from multiple Weyl nodes in high-mobility $EuTiO_3$ films, Sci. Adv. **4**, eaar7880 (2018).

[14] K. Ahadi, Z. Gui, Z. Porter, J. W. Lynn, Z. Xu, S. D. Wilson, A. Janotti, and S. Stemmer, Carrier density control of magnetism and Berry phases in doped $EuTiO_3$, APL Mater. **6**, 056105 (2018).

[15] See Supplemental Material at http://link.aps.org/supplemental/10.1103/PhysRevResearch.3.L042038 for details on the samples deposition, structural, and magnetic characterization, on the ARPES data analysis and fitting, and supplementary DFT + U calculations.

[16] N. C. Plumb, M. Salluzzo, E. Razzoli, M. Mansson, M. Falub, J. Krempasky, C. E. Matt, J. Chang, M. Schulte, J. Braun, H. Ebert, J. Minar, B. Delley, K. J. Zhou, T. Schmitt, M. Shi, J. Mesot, L. Patthey, and M. Radovic, Mixed Dimensionality of Confined Conducting Electrons in the Surface Region of $SrTiO_3$, Phys. Rev. Lett. **113**, 086801 (2014).

[17] Z. Wang, S. M. Walker, A. Tamai, Y. Wang, Z. Ristic, F. Y. Bruno, A. de la Torre, S. Ricco, N. C. Plumb, M. Shi, P. Hlawenka, J. Sanchez-Barriga, A. Varykhalov, T. K. Kim, M. Hoesch, P. D. C. King, W. Meevasana, U. Diebold, J. Mesot, B. Moritz *et al.*, Tailoring the nature and strength of electron-phonon interactions in the $SrTiO_3$(001) 2D electron liquid, Nat. Mater. **15**, 835 (2016).

[18] N. C. Plumb, M. Kobayashi, M. Salluzzo, E. Razzoli, C. E. Matt, V. N. Strocov, K. J. Zhou, M. Shi, J. Mesot, T. Schmitt, L. Patthey, and M. Radovic, Evolution of the $SrTiO_3$ surface

electronic state as a function of $LaAlO_3$ overlayer thickness, Appl. Surf. Sci. **412**, 271 (2017).

[19] S. Muff, M. Fanciulli, A. P. Weber, N. Pilet, Z. Ristic, Z. Wang, N. C. Plumb, M. Radovic, and J. H. Dil, Observation of a two-dimensional electron gas at $CaTiO_3$ film surfaces, Appl. Surf. Sci. **432**, 41 (2016).

[20] G. Kresse and J. Hafner, *Ab initio* molecular dynamics for liquid metals, Phys. Rev. B **47**, 558 (1993).

[21] G. Kresse and J. Furthmuller, Efficiency of *ab-initio* total energy calculations for metals and semiconductors using a plane-wave basis set, Comput. Mater. Sci. **6**, 15 (1996).

[22] P. E. Blochl, Projector augmented-wave method, Phys. Rev. B **50**, 17953 (1994).

[23] G. Kresse and D. Joubert, From ultrasoft pseudopotentials to the projector augmented-wave method, Phys. Rev. B **59**, 1758 (1999).

[24] J. P. Perdew, A. Ruzsinszky, G. I. Csonka, O. A. Vydrov, G. E. Scuseria, L. A. Constantin, X. Zhou, and K. Burke, Restoring the Density-Gradient Expansion for Exchange in Solids and Surfaces, Phys. Rev. Lett. **100**, 136406 (2008).

[25] S. L. Dudarev, G. A. Botton, S. Y. Savrasov, C. J. Humphreys, and A. P. Sutton, Electron-energy-loss spectra and the structural stability of nickel oxide: An LSDA+U study, Phys. Rev. B **57**, 1505 (1998).

[26] M. Breitschaft, V. Tinkl, N. Pavlenko, S. Paetel, C. Richter, J. R. Kirtley, Y. C. Liao, G. Hammerl, V. Eyert, T. Kopp, and J. Mannhart, Two-dimensional electron liquid state at $LaAlO_3$-$SrTiO_3$ interfaces, Phys. Rev. B **81**, 153414 (2010).

[27] I. I. Piyanzina, Y. V. Lysogorskiy, I. I. Varlamova, A. G. Kiiamov, T. Kopp, V. Eyert, O. V. Nedopekin, and D. A. Tayurskii, Analysis of electronic and structural properties of surfaces and interfaces based on $LaAlO_3$ and $SrTiO_3$, J. Low Temp. Phys. **185**, 597 (2016).

[28] H. O. Jeschke, J. Shen, and R. Valentí, Localized versus itinerant states created by multiple oxygen vacancies in $SrTiO_3$, New J. Phys. **17**, 023034 (2015).

[29] M. Altmeyer, H. O. Jeschke, O. Hijano-Cubelos, C. Martins, F. Lechermann, K. Koepernik, A. F. Santander-Syro, M. J. Rozenberg, R. Valenti, and M. Gabay, Magnetism, Spin Texture, and In-Gap States: Atomic Specialization at the Surface of Oxygen-Deficient $SrTiO_3$, Phys. Rev. Lett. **116**, 157203 (2016).

[30] A. F. Santander-Syro, F. Fortuna, C. Bareille, T. C. Roedel, G. Landolt, N. C. Plumb, J. H. Dil, and M. Radovic, Giant spin splitting of the two-dimensional electron gas at the surface of $SrTiO_3$, Nat. Mater. **13**, 1085 (2014).

[31] S. McKeown Walker, S. Riccò, F. Y. Bruno, A. de la Torre, A. Tamai, E. Golias, A. Varykhalov, D. Marchenko, M. Hoesch, M. S. Bahramy, P. D. C. King, J. Sanchez-Barriga, and F. Baumberger, Absence of giant spin splitting in the two-dimensional electron liquid at the surface of $SrTiO_3$ (001), Phys. Rev. B **93**, 245143 (2016).

[32] Z. Gui and A. Janotti, Carrier-Density-Induced Ferromagnetism in $EuTiO_3$ Bulk and Heterostructures, Phys. Rev. Lett **123**, 127201 (2019).

[33] D. Stornaiuolo, C. Cantoni, G. M. De Luca, R. Di Capua, E. Di Gennaro, G. Ghiringhelli, B. Jouault, D. Marre, D. Massarotti, F. M. Granozio, I. Pallecchi, C. Piamonteze, S. Rusponi, F. Tafuri, and M. Salluzzo, Tunable spin polarization and superconductivity in engineered oxide interfaces, Nat Mater. **15**, 278 (2016).

[34] F. Gunkel, C. Bell, H. Inoue, B. Kim, A. G. Swartz, T. A. Merz, Y. Hikita, S. Harashima, H. K. Sato, M. Minohara, S. Hoffmann-Eifert, R. Dittmann, and H. Y. Hwang, Defect Control of Conventional and Anomalous Electron Transport at Complex Oxide Interfaces, Phys. Rev. X **6**, 031035 (2016).

[35] X. Cai, J. Yue, P. Xu, B. Jalan, and V. S. Pribiag, From weak antilocalization to Kondo scattering in a magnetic complex oxide interface, Phys. Rev. B **103**, 115434 (2021).